International Journal of Solids and Structures 302 (2024) 112992



Contents lists available at ScienceDirect

International Journal of Solids and Structures

journal homepage: www.elsevier.com/locate/ijsolstr



Torsional buckling of a tape-spring: Review and renew

J.A. Clarkson, K.A. Seffen *

Advanced Structures Group, Department of Engineering, University of Cambridge, Cambridge CB2 1PZ, UK

ARTICLE INFO

Keywords:
Tape-spring
Deployable structures
Shell
Torsional buckling
Approximate solutions
Rayleigh–Ritz

ABSTRACT

Tape-springs – straight strips with transversely curved cross-sections – undergo a flattening of the cross-section upon bending, and accompanying torsional buckling in equal-sense bending which then "recedes" at greater deformation. The exact analytical solution for tape-spring bending was solved by Mansfield; however, the resulting expression for the twisting curvature at the onset and recession of torsional buckling cannot be solved in closed-form. Approximate closed-form expressions are therefore sought: firstly, by utilising Taylor series approximations of Mansfield's extensive functions; and secondly, by assuming a uniform transverse curvature, thereby rendering the problem algebraic in nature, and deriving new governing expressions. Further approximations assume the cross-section does not deform upon bending, and that the tape-spring remains a developable surface in the inextensible limit of zero thickness. All approximate solutions are shown to agree closely with Mansfield's solution at small curvatures, with the uniform curvature approximation also capturing the recession of torsional buckling to a reasonable degree of accuracy. The accuracy of the uniform curvature approximation is related to a pertinent dimensionless parameter, which governs the size of a boundary layer in Mansfield's exact solution: as this parameter tends to infinity, the uniform curvature approximation and Mansfield's exact solution are shown to converge; as it tends to zero, all solutions are shown to converge on the inextensible limit.

1. Introduction

Tape-springs are a class of straight strips with transversely curved cross-sections, with the tape-measure, *viz.* carpenter's tape, being the most familiar. Its relatively high bending stiffness ensures that a long tape deflects minimally under self-weight, just as the carpenter's tape performs over typical household distances. Tape-springs are also highly deformable: an over-extended carpenter's tape generates an excessive root bending moment before locally collapsing into a concentrated cylindrical hinge next to its housing, which, incidentally, is the stowed configuration of tape inside.

Such different properties of high straight stiffness and compact "coilability" have promoted tape-springs to significant applications involving deployable structures (Miura and Pellegrino, 2020). The original proponent was F P J Rimrott, a Canadian academic and Aerospace Engineer, who developed the concept of the storable tubular extendible member, or "STEM", in 1965 as a deployable boom for spacecraft (Rimrott, 1965); as a communications antenna or for gravity compensation (and, thus, attitude control) by adjusting the relative position of a tip-mass in orbit.

The cross-section of a STEM typically subtends just over one full turn of an open, overlapping circle—more than six times the angle ($\approx 60°$) subtended by the usual carpenter's tape; and remains open in order to become flattened before coiling onto a motorised deployment hub. Being open, however, predicates a lower torsional stiffness compared to a closed cross-section (Rimrott, 1970), which makes a STEM liable to coupled torsional buckling when compressed axially, for example: as happened in the pair of STEMS supporting a solar array on the Hubble Space Telescope (Thornton et al., 1998).

Shortly after Rimrott's STEM proposal, E H Mansfield delivered, in 1973, a consummate study on the deformation of the more traditional "shallow" tape-spring, but now possibly curved along its length initially, as in a bicycle mudguard, or twisted, propeller-like (Mansfield, 1973). In dealing with "strips", which Mansfield deemed to be narrow lengths of curved shell, he was able to curate a variety of shell-like behaviour, now eminently tractable because their bending and stretching actions were dominant in single, respectively orthogonal directions, as in traditional cylindrical shell behaviour—a moderately simpler specialisation of shell theory, in general (Calladine, 1983); furthermore, the deformation was *uniformly* cast along the strip in response to equal and opposite moments, M, and/or torques, T, applied to its ends (with no length-wise variation of initial curvatures).

In order to solve the corresponding fourth-order governing equation of cross-sectional displacements with the correct boundary conditions, Mansfield cannily employed a cross-section with a thickness that tapered to zero on both sides. The provision of "free" longitudinal edges

* Corresponding author.
E-mail addresses: jac287@cam.ac.uk (J.A. Clarkson), kas14@cam.ac.uk (K.A. Seffen).

https://doi.org/10.1016/j.ijsolstr.2024.112992
Received 6 June 2024; Received in revised form 14 July 2024; Accepted 17 July 2024
Available online 19 July 2024
0020-7683/© 2024 The Authors. Published by Elsevier Ltd. This is an open access article under the CC BY license (http://creativecommons.org/licenses/by/4.0/).

is now satisfied automatically, and the particular quadratic variation of thickness, which gives rise to a lens-like, or *lenticular*, cross-section, precisely metes the required variation within the governing differential equation. There is, consequently, a viable *algebraic* root for the unknown *uniform* transverse curvature of the deformed cross-section in terms of the length-wise deformation curvatures, amongst other initial terms, now ''responsible for the relative simplicity of the ensuing analysis'' in Mansfield's words.

Full expressions for the moment–curvature and torque-twisting responses are obtained in closed form, which directly convey their high degree of nonlinearity and, thus, potentially diverse behaviour: from peak loading and early "snap-through" buckling to asymptotic linear behaviour when the deformed strip garners a *developable* shape at larger displacements (Calladine, 1983).

The algebraic convenience also affords definitive statements about any possible interaction between the responses, in particular, the occurrence of torsional buckling during flexure: Mansfield furnishes the requisite relationships concerning the initial shape of strips, the deformation range over which the bucking mode prevails and, crucially, the corresponding applied buckling moment, which turns out to be constant throughout.

Mansfield deals with "constant-thickness" strip behaviour in a final act, which turns out to have more complex response expressions replete with hyperbolic functions. The latter conflate an exact solution that reproduces the narrow boundary layers along both free edges over which stress resultants attenuate to zero: the bulk of the deformed cross-section is otherwise uniformly curved.

Torsional-flexural buckling is easily demonstrated when a length of carpenter's tape is bent such that longitudinal curving induces compression along the free edges: this is known as "equal-sense" bending since the induced curvature is in the same sense as the original transverse curvature. The onset of buckling occurs almost immediately, without any discernible cross-sectional deformation; rather, twisting along the tape is initiated by a rigid-body rotation of the middle cross-section. Turning the tape-spring over and bending with "opposite-sense" curvature, the cross-section flattens in a manner similar to Brazier's ovalisation in pipes (Brazier, 1926), before eventually snapping without any twisting.

The analysis of both modes of buckling for constant-thickness strips proceeds as per lenticular strips, but solving for the corresponding applied moments in closed form is stymied by the inevitable hyperbolic terms, which are also functions of the longitudinal curvature: Mansfield develops a numerical solution by referring to tabulated values in Mansfield (1973).

Moving forward, the use of curved strips, *viz.* tape-springs for creating lightweight and highly deformable elements in spacecraft and aerospace applications–as per Rimrott's foresight, has been revitalised over the last twenty-five years, now manufactured from materials other than metals such as fibre-composite laminates. The ability to tailor specific orthotropic properties further unlocks the scope for novel behaviour, for example, *bistable* fibre-composite shells with two, distinct cylindrical shapes, which do not rely on auxiliary production processes such as pre-stressing (Iqbal et al., 2000); moving between bistable states, reversibly, is enabled by large elastic deformability.

The extra constitutive material information, of course, increases the overall parameter specification: a Mansfield-type exact analysis is feasible but has more corresponding detail, *e.g.* see Galletly and Guest (2004). However, it was apparent that the equilibrium *scope* of these bistable shells did not depend on the marshalling loads (Guest and Pellegrino, 2006), just as related developments in more general multistable shells were emerging, based on approximate but compact descriptions of deformation (Seffen, 2009; Vidoli and Maurini, 2008). Their viability stems from the influence of shell thickness—or, rather, thinness, which promotes two simplifying practical adjustments: diminishing boundary-layer widths and "middle-surface" *i.e.* in-plane forces.

The shape of a relatively thin, deforming tape-spring can therefore reasonably neglect its very narrow boundary layers from the outset, where adopting a non-varying, uniform and, hence, simpler distribution of deformation curvatures, is prescient. The governing differential equation no longer applies, and the loading response is found from the stationary performance of an algebraic potential formulated in terms of the curvatures, which must include the action of middle-surface forces otherwise buckling is precluded; these forces approach zero as the deformed shape becomes developable under large enough displacements.

We therefore revisit the fundamental deformation response of curved strips under these assumptions, which, to our knowledge, has not been explored. Torsional-flexural buckling is of primary interest because of the increased analytical scope from mode-coupling and because Mansfield's prediction of the corresponding moment must ultimately be solved numerically. Torsion-related outcomes from coupled buckling in general are more difficult to anticipate—as per the Hubble Space Telescope, and are often regarded as "invidious" because they dramatically undercut any prospective capacity from the primary deformation mode, which will be evident from, first, replaying Mansfield's exact solution.

The onset of buckling has been a priority in other studies (Wang et al., 2019): recovery has not been—which occurs at much higher deformation. The analysis of WJ Supple (Supple, 1969) is an early example of systems that buckle into a mode-shape before returning to the original deformation at a higher load; but these are simple systems in discrete variables, with little follow up in the literature that is not obvious. For ordinary tape-springs, it is difficult to disentangle such recovery from localisation of the tape-spring into a fold; thus, we leave the problem of fold-torsion interaction for now, and consider purely uniform length-wise deformations.

We will show that wide-ranging nonlinear variation is controlled by a pertinent dimensionless group, which is also related to the overall accuracy in our approach. Our "uniform curvature" analysis then follows where we, first, allow for uniform changes in curvature, before simplifying further by fixing the transverse curvature to its initial value. A final uniform curvature model assumes fully developable behaviour.

2. Analytical scope of study

This study begins with Mansfield's exact analysis of the bending and torsion of a constant-thickness tape-spring. The behaviour is fully coupled and nonlinear: curving and twisting can stem from the application of equal and opposite bending moments *and* torques.

Mansfield determines the case for buckling from bending into a coupled twisting mode without torque by solving for non-zero twisting curvature, κ_{xy}, ultimately as a function of the longitudinal curvature, κ_x. Torsional buckling turns out to be a feature of equal-sense bending, but not all tape-spring geometries are amenable.

The torsional mode is declared by Mansfield to be "preferred" because of a reduction in the applied bending moments compared to the case without twisting: more formally it can be shown that the zero-twist solution is an unstable equilibrium versus a stable equilibrium in the torsional mode. The onset of torsional buckling occurs when κ_{xy} is zero in the κ_x function; however, the hyperbolic functions do not avail an exact solution in closed form. Approximate versions are therefore desirable, at the very least.

Noting that initiating values of κ_x are typically relatively small, a first approach considers Taylor-series expansions of Mansfield's hyperbolic functions. The onset of torsional buckling is usefully captured; however, the point at which buckling recedes – an exceptional property of tape-springs at much larger curvatures – is not.

In general, the deformed cross-section has uniform transverse curvature except for narrow boundary layers close to the free edges, over which the corresponding bending moment rapidly attenuates, commensurate with hyperbolic functions (in part: they also describe

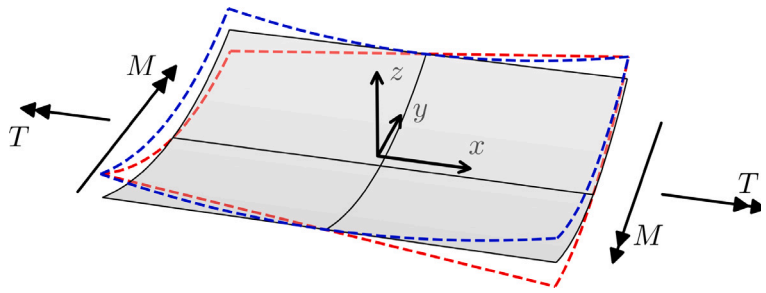


Fig. 1. The coordinate system adopted in this paper, which is consistent with that used by Mansfield. Curvature is defined such that $\kappa_x = d^2z/dx^2$, with positive κ_x and κ_{xy} illustrated by dashed blue and red outlines respectively. The vectors M and T, following a right-hand screw rule, identify positive equal-sense bending moments, and torque.

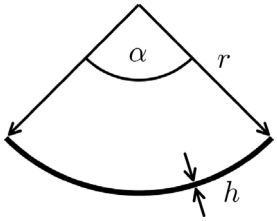


Fig. 2. Tape-spring cross-section geometry.

the largely constant bulk shape). Compromising accuracy for simplicity, the differential nature of the problem is dispatched by ignoring the boundary layer effect and focussing on bulk *uniform* deformation, which is treated by an algebraic energetic approach.

In the first case, the uniform transverse curvature is allowed to vary, for a greater range of deformation, including when buckling recedes. Second, the transverse curvature is assumed to be uniform and fixed, which is reasonable only for small curvatures and for predicting the onset of torsional buckling. Finally, inextensible, developable behaviour is assumed, valid in the limit of zero thickness. The influence of the boundary layer and the accuracy of the approximate solutions, which are directly related, can be tracked via a relevant dimensionless group, as noted.

3. Mansfield's constant thickness analysis

Orthogonal coordinates, (x, y), are respectively aligned to the longitudinal and transverse directions of a thin strip, which has initial uniform curvatures, $\kappa_{x,0}$ and $\kappa_{y,0}$, with uniform twisting curvature, $\kappa_{xy,0}$. The Young's modulus is E, shear modulus, G, and Poisson's ratio, ν; the constant thickness of strip is h, and the cross-section subtends an angle α such that the transverse arc-width is $b = r\alpha$, where $r = 1/\kappa_{y,0}$ (see Fig. 2).

Equal and opposite moments, M, applied to the ends of strip produce a uniform longitudinal curvature, κ_x: when κ_x is in the same direction as $\kappa_{y,0}$, we have "equal-sense" bending; otherwise, it is declared to be "opposite-sense". Similarly, for equal and opposite torques applied axially, T, there is a new twisting curvature, κ_{xy}, with the notation for both shown in Fig. 1.

Mansfield (1973) proposes that every cross-section along the tape distorts the same, with out-of-plane displacements normal to x and y being governed by a differential equation of cylindrical shell bending, which relates dominant transverse bending moments and longitudinal in-plane forces. The equation can be solved exactly, with ultimate expressions for each of the loading responses (subscript denominated) as:

$$\bar{M}_{\text{Mansf}} = \bar{\kappa}_x - \bar{\kappa}_{x,0} + \frac{\Lambda}{1-\nu^2}\left[\tau\Psi_1(\bar{\kappa}_x) - \Lambda\bar{\kappa}_x\Psi_2(\bar{\kappa}_x)\right] \tag{1}$$

$$\bar{T}_{\text{Mansf}} = \bar{\kappa}_{xy} - \bar{\kappa}_{xy,0} + \frac{\Lambda}{1-\nu}\bar{\kappa}_{xy}\Psi_1(\bar{\kappa}_x) \tag{2}$$

where the "over-barred" moment, torque and curvature are dimensionless parameters according to

$$\bar{M} = \frac{3b\sqrt{3(1-\nu^2)}}{Eh^4}M, \bar{T} = \frac{3b\sqrt{3(1-\nu^2)}}{4Gh^4}T, \quad \bar{\kappa} = \frac{b^2\sqrt{3(1-\nu^2)}}{4h}\kappa \tag{3}$$

Their nonlinear coupling at larger displacements proceeds from the common parameter, Λ, which is defined to be

$$\Lambda = \bar{\kappa}_{xy}^2 - \bar{\kappa}_{xy,0}^2 + (\bar{\kappa}_x - \bar{\kappa}_{x,0})(\nu\bar{\kappa}_x - \bar{\kappa}_{y,0}) \tag{4}$$

with τ, another auxiliary parameter, as

$$\tau = 2\nu\bar{\kappa}_x - \bar{\kappa}_{y,0} - \nu\bar{\kappa}_{x,0} \tag{5}$$

and, finally, Ψ_1 and Ψ_2, as detailed functions of $\bar{\kappa}_x$, including hyperbolic terms

$$\Psi_1(\bar{\kappa}_x) = \frac{1}{\bar{\kappa}_x^2}\left[1 - \frac{1}{\sqrt{\bar{\kappa}_x}}\frac{\cosh(2\sqrt{\bar{\kappa}_x}) - \cos(2\sqrt{\bar{\kappa}_x})}{\sinh(2\sqrt{\bar{\kappa}_x}) + \sin(2\sqrt{\bar{\kappa}_x})}\right] \tag{6}$$

$$\Psi_2(\bar{\kappa}_x) = \frac{1}{\bar{\kappa}_x^4}\left[1 + \frac{\sinh(2\sqrt{\bar{\kappa}_x})\sin(2\sqrt{\bar{\kappa}_x})}{(\sinh(2\sqrt{\bar{\kappa}_x}) + \sin(2\sqrt{\bar{\kappa}_x}))^2} - \frac{5}{4\sqrt{\bar{\kappa}_x}}\frac{\cosh(2\sqrt{\bar{\kappa}_x}) - \cos(2\sqrt{\bar{\kappa}_x})}{\sinh(2\sqrt{\bar{\kappa}_x}) + \sin(2\sqrt{\bar{\kappa}_x})}\right] \tag{7}$$

Consider pure bending with no torque applied for the case of an untwisted strip initially, as Mansfield does. Setting the right-hand side of Eq. (2) equal to zero, we find two roots

$$\bar{\kappa}_{xy}\left[1 - \nu + \Lambda\Psi_1(\bar{\kappa}_x)\right] = 0 \quad \Rightarrow \quad \bar{\kappa}_{xy} = 0, \quad 1 - \nu + \Lambda\Psi_1 = 0 \tag{8}$$

The first root complies with pure *curving* under M. For standard straight tape-springs ($\kappa_{x,0} = 0$, $\kappa_{xy,0} = 0$, $\kappa_{y,0} = 1/r$), the zero-twist moment can be written in an alternative dimensionless form as

$$\frac{Mr}{Db} = (\kappa_x r - \nu) + \nu\left(1 - \nu\kappa_x r\right)P_1(\bar{\kappa}_x) + \frac{\left(1-\nu\kappa_x r\right)^2}{\kappa_x r}P_2(\bar{\kappa}_x) \tag{9}$$

where

$$P_1(\bar{\kappa}_x) = 1 - \bar{\kappa}_x^2\Psi_1(\bar{\kappa}_x), \quad P_2(\bar{\kappa}_x) = \bar{\kappa}_x^2\Psi_1(\bar{\kappa}_x) - \bar{\kappa}_x^4\Psi_2(\bar{\kappa}_x)$$

and D is the plate flexural rigidity, $Eh^3/12(1-\nu^2)$. Eq. (9) is perhaps a more useful dimensionless representation than Mansfield's choice, because there is an immediate sense of the likely range of $\kappa_x r$, from 0 to 1: when $\kappa_x r = \pm 1$, i.e. $\kappa_x = \pm 1/r$, the longitudinal curvature is equal to the initial transverse curvature, which is precisely the curvature of the buckled cylindrical hinge, or "fold", that forms (Rimrott, 1970); the properties of tape-spring folds are well established and are covered elsewhere (Clarkson and Seffen, 2024). It should be noted that Eq. (9) is identical to an earlier analytical solution for tape-spring bending derived by Wuest (1954), who did not consider torsional effects.

The second root allows for twisting from torsional buckling observed during equal-sense bending. Rearranging the root leads to an explicit expression for the twist:

$$\bar{\kappa}_{xy}^2 = \bar{\kappa}_x(\bar{\kappa}_{y,0} - \nu\bar{\kappa}_x) - \frac{1-\nu}{\Psi_1(\bar{\kappa}_x)} \tag{10}$$

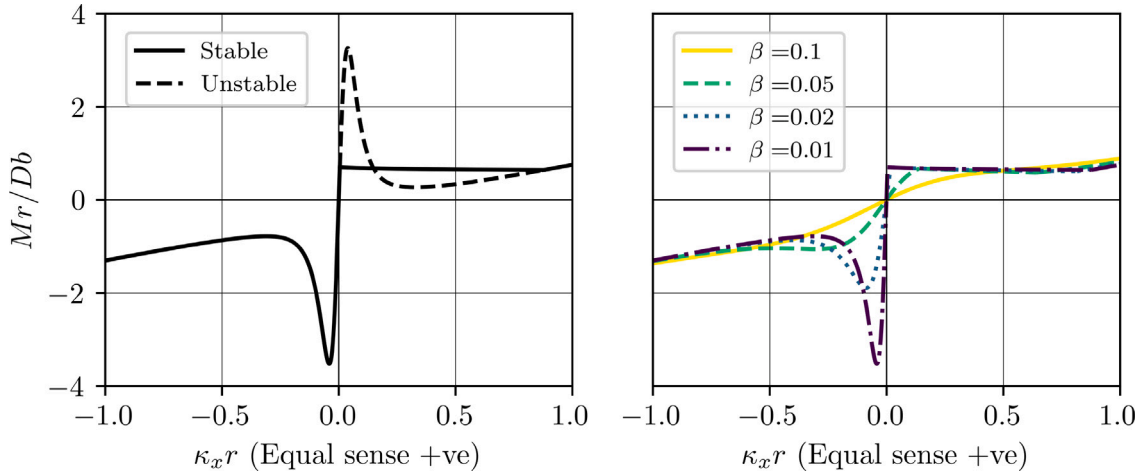


Fig. 3. On the left, the Mansfield solution, with stable and unstable paths: the zero-twist moment, Eq. (9), is the single, stable, solution for most κ_x, but unstable over the range of positive κ_x in which the torsional buckling solution, Eq. (12), exists. On the right, the stable path is plotted for a range of β.

Torsional buckling can therefore only occur over the range in which $\bar{\kappa}_{xy}^2$ is positive, which is some range of positive $\bar{\kappa}_x$ depending on the value of $\bar{\kappa}_{y,0}$: the exact range requires a numerical solution. The corresponding moment is tractable, nevertheless

$$\bar{M} = \frac{\bar{\kappa}_{y,0} - \bar{\kappa}_{x,0}}{1+\nu} + \bar{\kappa}_x \left(\frac{1-\nu}{1+\nu}\right)\left(1 - \frac{\Psi_2(\bar{\kappa}_x)}{\Psi_1^2(\bar{\kappa}_x)}\right) \tag{11}$$

and can be written in the alternate dimensionless form for a straight tape-spring as:

$$\frac{Mr}{Db} = 1 - \nu + \kappa_x r(1-\nu)^2 \left(1 - \frac{\Psi_2(\bar{\kappa}_x)}{\Psi_1^2(\bar{\kappa}_x)}\right) \tag{12}$$

By plotting Mr/Db against $\kappa_x r$, it can be seen that the form of Eq. (9) & (12) depend only on ν and $\bar{\kappa}_x$. Rewriting $\bar{\kappa}_x$ to include r:

$$\bar{\kappa}_x = \frac{b^2\sqrt{3(1-\nu^2)}}{4hr}\kappa_x r \tag{13}$$

reveals that $\bar{\kappa}_x$, and, hence, $\Psi_1 \& \Psi_2$, depend on ν, the dimensionless curvature $\kappa_x r$, and a parameter ratio:

$$\beta = \frac{rh}{b^2} \tag{14}$$

which can be thought of as the product of $1/\alpha$ (= r/b) and h/b, *i.e.* the "flatness" times the relative thickness. As β increases, the tape-spring becomes flatter and thicker, and more "plate-like"; as β decreases the tape-spring becomes more characteristically "shell-like". Unsurprisingly, this parameter has appeared in previous work: Calladine & Seffen's analysis of tape-spring folds (Calladine and Seffen, 2020) presents the analogous $T = \alpha\sqrt{r/h} = 1/\sqrt{\beta}$; moreover, it is essentially the Batdorf parameter for curved plates (Batdorf, 1947), $Z = \sqrt{1-\nu^2}b^2/rh$. It is also closely related to the characteristic curvature strain, $\bar{\kappa}$, presented by Audoly and Neukirch (2021), in the context of dimension reduction for elastic ribbons of length L: $\bar{\kappa} = b^2/Lh$.

Thus, the dimensionless moment is only a function of $\kappa_x r$, β and ν, where Fig. 3 plots the stable and unstable moment–curvature solutions for $\nu = 0.3$ and a range of β. In equal-sense bending, the moment under zero twist, Eq. (9), is similar to opposite-sense bending, but is unstable over a range of $\kappa_x r$ where it buckles torsionally at a small curvature moment before the unstable peak. The torsional buckling moment, Eq. (12), is nearly constant as the twist increases then decreases to zero close to $\kappa_x r = 1$, reverting to the zero-twist stable bending. It is evident that the torsional buckling moment has little dependence on either β or $\kappa_x r$.

Generally, smaller β tape-springs have a stiffer initial response and greater peak moment in opposite-sense bending: tape-springs with larger β have a smaller peak moment occurring at a larger non-dimensional curvature; and tape-springs with greatest β have little to no peak moment at all. Thus, the value of β captures the degree to which the behaviour is tape-spring-like: small β results in a significant peak and softening behaviour, while large β behaviour is barely distinguishable from that of a plate. For practical tape-springs, b/h might reasonably range between 50 and 300, and $b/r = \alpha$ might reasonably range between $\pi/6$ and $\pi/2$, giving a rough range of practical β between 0.002 and 0.04. It would be eminently feasible to manufacture tape-springs with arbitrarily large β, but the increasingly plate-like response renders them indifferent to a flat strip, at which point they cease to be usefully described as tape-springs.

4. Approximate solutions

4.1. Approximating Mansfield's solution

Mansfield's exact solution cannot provide a closed form solution for the twist onset of torsional buckling due to the trigonometric expressions in $\Psi_1(\bar{\kappa}_x)$ in Eq. (10): therefore, as a first step, one may consider $\Psi_1(\bar{\kappa}_x)$ as the first terms of a Taylor Series, with receding higher-order terms because $\bar{\kappa}_x$ is small when torsional buckling occurs: therefore expansion

$$\Psi_1(\bar{\kappa}_x) = \frac{4}{45} - \frac{32}{2835}\bar{\kappa}_x^2 + \mathcal{O}\left(\bar{\kappa}_x^4\right) \tag{15}$$

It should be noted that this corresponds to the leading order prediction in an asymptotic dimension reduction of tape-springs performed by Kumar et al. (2023).

However, $\bar{\kappa}_x$ increases with slenderness b/h, thus it is also useful to consider the extreme limit as $\bar{\kappa}_x \to \infty$:

$$\lim_{\bar{\kappa}_x \to \infty} \Psi_1(\bar{\kappa}_x) = \frac{1}{\bar{\kappa}_x^2} \tag{16}$$

Fig. 4 plots these two approximations alongside Ψ_1 exactly; the small $\bar{\kappa}_x$ approximation appears reasonable below $\bar{\kappa}_x \approx 1$, and the large $\bar{\kappa}_x$ approximation reasonable above $\bar{\kappa}_x \approx 10$. But note, that, for thin tape-springs, large b/h increases $\bar{\kappa}_x$ for a given κ_x; this potentially counteracts the expected small value of κ_x at the onset of torsional buckling. Thus, it is not immediately obvious which, if any, Ψ_1 approximation will be appropriate; nevertheless, we proceed assuming the small $\bar{\kappa}_x$ approximation is valid, which we will check after obtaining predicted values of $\bar{\kappa}_x$.

Substituting Eq. (15) in to Eq. (10), setting $\bar{\kappa}_{xy}^2 = 0$, and multiplying out yields a quartic in $\bar{\kappa}_x$:

$$0 = \frac{32}{2835}\nu\bar{\kappa}_x^4 - \frac{32}{2835}\bar{\kappa}_{y,0}\bar{\kappa}_x^3 - \frac{4}{45}\nu\bar{\kappa}_x^2 + \frac{4}{45}\bar{\kappa}_{y,0}\bar{\kappa}_x - 1 + \nu \tag{17}$$

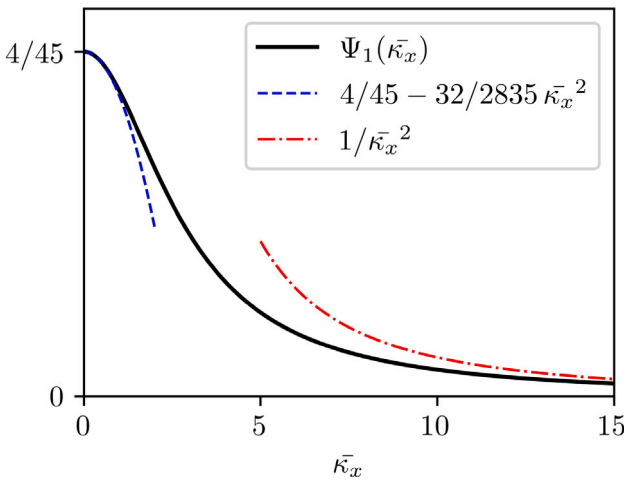


Fig. 4. Approximations of $\Psi_1(\bar{\kappa_x})$, Eq. (6) (exact) by simplified expressions.

This can also be written in terms of the dimensionless curvature $\kappa_x r$:

$$0 = \frac{8\nu(1-\nu^2)}{21}(\kappa_x r)^4 - \frac{8(1-\nu^2)}{21}(\kappa_x r)^3 - 16\nu\beta^2(\kappa_x r)^2 + 16\beta^2\kappa_x r - \frac{960\beta^4}{(1+\nu)} \tag{18}$$

where we see the dimensionless parameter β appear again. If Eq. (15) is curtailed to the constant term, the quartic becomes a quadratic:

$$0 = \nu(\kappa_x r)^2 - \kappa_x r + \frac{60\beta^2}{(1+\nu)} \tag{19}$$

Finally, assuming κ_x to be small, one can obtain a linear approximation

$$\kappa_x r = \frac{60\beta^2}{(1+\nu)} \tag{20}$$

Reverting to Mansfield's dimensionless form, this can be written as

$$\bar{\kappa}_x = 15\sqrt{\frac{3(1-\nu)}{(1+\nu)}}\beta \tag{21}$$

For most tape-springs $\nu \approx 0.3$, thus $\bar{\kappa}_x \approx 19\beta$. Given the Ψ_1 power series approximation is valid for $\bar{\kappa}_x < 1$, the buckling onset curvature prediction will be valid for all tape-springs with $\beta < 1/19 \approx 0.05$, which covers the majority of tape-springs. Importantly, it indicates that thinner tape-springs buckle at smaller $\bar{\kappa}_x$, and so the small $\bar{\kappa}_x$ approximation not only remains valid but actually increases in accuracy as β decreases.

In contrast to the onset curvature, Mansfield's closed-form expression for the torsional buckling moment, Eq. (11), contains a (Ψ_2/Ψ_1^2): this is unwieldy and usefully approximated by invoking another Taylor series, about zero, which is found to be:

$$\frac{\Psi_2(\bar{\kappa}_x)}{\Psi_1(\bar{\kappa}_x)^2} = \frac{10}{7} - \frac{152}{63063}\bar{\kappa}_x^2 + \mathcal{O}\left(\bar{\kappa}_x^4\right) \tag{22}$$

Truncating at the constant term, and substituting into Eq. (12) leads to a compact approximation

$$\frac{Mr}{Db} = (1-\nu) - \frac{3}{7}(1-\nu)^2\kappa_x r \tag{23}$$

For the eventual vanishing of the torsional buckling mode, c.f. Fig. 3, we can substitute the large $\bar{\kappa}_x$ approximation, Eq. (16), into Eq. (10), assuming a very thin tape-spring, to obtain:

$$\begin{aligned}\bar{\kappa}_{xy}^2 &= \bar{\kappa}_x(\bar{\kappa}_{y,0} - \nu\bar{\kappa}_x) - (1-\nu)\bar{\kappa}_x^2 \\ &= \bar{\kappa}_x(\bar{\kappa}_{y,0} - \bar{\kappa}_x)\end{aligned} \tag{24}$$

Setting $\bar{\kappa}_{xy}^2 = 0$ leads to roots $\bar{\kappa}_x = 0$ and $\bar{\kappa}_x = \bar{\kappa}_{y,0}$; additionally, the large $\bar{\kappa}_x$ limit of Ψ_2/Ψ_1^2 is

$$\lim_{\bar{\kappa}_x \to \infty} \frac{\Psi_2(\bar{\kappa}_x)}{\Psi_1(\bar{\kappa}_x)^2} = 1 \tag{25}$$

resulting in the final the torsional buckling moment as equal to

$$\frac{Mr}{Db} = 1 - \nu \tag{26}$$

which exactly corresponds to the equal-sense fold moment: why this is so, and whether or not there is underlying coupling between the two instabilities, is currently being studied.

Fig. 4 shows that the large $\bar{\kappa}_x$ approximation converges fairly slowly, so Eq. (24) will only become accurate as b/h tends to very large values (as $\beta \to 0$).

In conclusion: approximating Mansfield's hyperbolic functions has provided some useful solutions, but no single expression which is valid over the whole range of $\bar{\kappa}_x$. Let us therefore derive alternative response expressions assuming, as discussed, a uniform transverse curvature across the cross-section.

4.2. Uniform curvature approximations

4.2.1. Strain energy formulation

The strain energy density for a shell in bending is written as Calladine (1983):

$$u_B = \frac{1}{2}D\left(\chi_x^2 + 2\nu\chi_x\chi_y + \chi_y^2 + 2(1-\nu)\chi_{xy}^2\right) \tag{27}$$

where χ_x, χ_y, χ_{xy} are the changes in curvature: for an initially straight tape-spring, $\chi_x = \kappa_x$, $\chi_y = \kappa_y - \kappa_{y0}$ and $\chi_{xy} = \kappa_{xy}$. The strain energy density due to in-plane strains of the shell mid-surface is

$$u_S = \frac{Eh}{2(1-\nu^2)}\left(\epsilon_x^2 + 2\nu\epsilon_x\epsilon_y + \epsilon_y^2\right) + \frac{E}{4(1+\nu)}\gamma_{xy}^2 \tag{28}$$

Assuming that longitudinal strains dominate the response, such that shear strains can be neglected, and that the transverse stress, σ_y, is zero such that $\epsilon_y = -\nu\epsilon_x$, the stretching energy density reduces to

$$u_S = \frac{Eh}{2}\epsilon_x^2 \tag{29}$$

The strain variation can be related to the change in Gaussian curvature, which is denoted as g in Calladine (1983):

$$g = \kappa_x\kappa_y - \kappa_{xy}^2 = -\frac{\partial^2\epsilon_x}{\partial y^2} + \frac{\partial^2\gamma_{xy}}{\partial x\partial y} - \frac{\partial^2\epsilon_y}{\partial x^2} \tag{30}$$

Since there is no x-wise variation of bending along the tape, the above simplifies to

$$\frac{\partial^2\epsilon_x}{\partial y^2} = -(\kappa_x\kappa_y - \kappa_{xy}^2) \tag{31}$$

which is a constant given the uniform terms in g. Integrating twice leads to

$$\epsilon_x = -(\kappa_x\kappa_y - \kappa_{xy}^2)\frac{y^2}{2} + Cy + D \tag{32}$$

Since, under pure bending, the "yaw" moment about an axis normal to the centroidal plane must be zero, by inspection the constant, C, is zero. Likewise, for no axial force, it is required that

$$Eh\int_{-b/2}^{b/2}\epsilon_x\,dy = 0 \tag{33}$$

which prescribes D, and the final strains to be:

$$\epsilon_x = (\kappa_{xy}^2 - \kappa_x\kappa_y)\left(\frac{y^2}{2} - \frac{b^2}{24}\right) \tag{34}$$

Substituting ϵ_x into u_S, Eq. (29), along with κ_x, κ_y and κ_{xy} into u_B, Eq. (27), we integrate across the width between limits, $y = \pm b/2$, assuming a shallow cross-section, to find:

$$\begin{aligned}U = \int_{-b/2}^{b/2} u_S + u_B\,dy = &\frac{Ehb^5}{1440}\left[\kappa_{xy}^4 - 2\kappa_{xy}^2\kappa_x\kappa_y + \kappa_x^2\kappa_y^2\right] \\ &+ \frac{Db}{2}\left[\kappa_x^2 + 2\nu\kappa_x(\kappa_y - \kappa_{y0}) + (\kappa_y - \kappa_{y0})^2 + 2(1-\nu)\kappa_{xy}^2\right]\end{aligned} \tag{35}$$

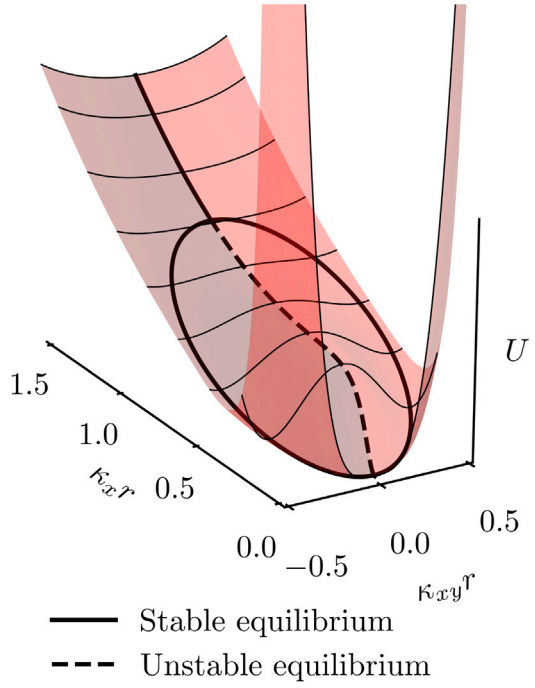


Fig. 5. Strain energy for $\beta = 0.01$.

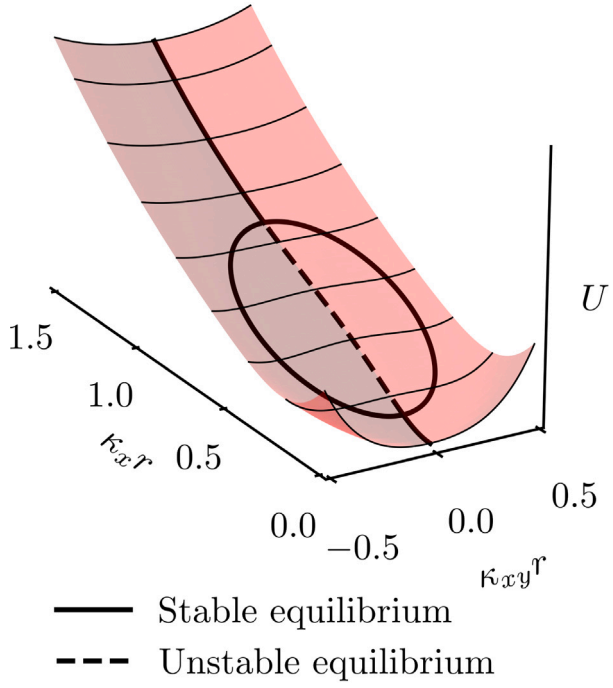


Fig. 6. Strain energy for $\beta = 0.05$.

4.2.2. First approximation—Solution UC1

We assume κ_y may vary as a function of κ_x and κ_{xy}, which necessitates minimising U, Eq. (35), with respect to κ_y first, i.e.:

$$\frac{\partial U}{\partial \kappa_y} = \frac{Ehb^5}{720}\left[-\kappa_{xy}^2\kappa_x + \kappa_x^2\kappa_y\right] + \frac{Db}{2}\left[2\nu\kappa_x + 2(\kappa_y - \kappa_{y0})\right] = 0 \tag{36}$$

For a compact solution for κ_y, we define

$$K = \frac{(1-\nu^2)}{60}\frac{b^4}{h^2} \tag{37}$$

which sets the solution of Eq. (36)

$$\kappa_y = \frac{K\kappa_{xy}^2\kappa_x + \kappa_{y0} - \nu\kappa_x}{\left[K\kappa_x^2 + 1\right]} \tag{38}$$

At this point it is instructive to visualise the "strain energy landscape", which we plot as a function of κ_x, which is for equal-sense only, and κ_{xy} for two different values of β in Figs. 5 and 6, with the equilibria annotated. In Fig. 5, it is apparent that over a range of κ_x the zero-twist solution is unstable; instead, there are two stable equilibrium with non-zero κ_{xy}, which is the torsional buckling solution. Outside this range, there is only one equilibrium solution, $\kappa_{xy} = 0$, which is, of course, stable. Increasing κ_x from zero, the stable path undergoes a "pitchfork bifurcation" (Thompson and Hunt, 1973) and then a *recombination*. Fig. 6, in comparison, has a much flatter energy landscape, with the unstable "bulge" less obvious, where the buckled solution exists over a smaller range of κ_x. Together, they suggest there is a critical β at which torsional buckling vanishes.

We now proceed to obtain algebraic expressions for the twist, moment and torque. The applied torque, T, is given by the absolute differential, first, then re-expressed in partial derivatives by the chain rule:

$$T = \left(\frac{dU}{d\kappa_{xy}}\right)_{\kappa_x} = \frac{\partial U}{\partial \kappa_{xy}} + \frac{\partial U}{\partial \kappa_y}\frac{\partial \kappa_y}{\partial \kappa_{xy}} \tag{39}$$

Since $\partial U/\partial \kappa_y = 0$, this reduces to

$$T = \frac{\partial U}{\partial \kappa_{xy}} = \frac{Ehb^5}{360}\left[\kappa_{xy}^3 - \kappa_{xy}\kappa_x\kappa_y\right] + Db\left[2(1-\nu)\kappa_{xy}\right] \tag{40}$$

Similarly, the applied moment, M, is given by

$$M = \frac{dU}{d\kappa_x} = \frac{\partial U}{\partial \kappa_x} + \frac{\partial U}{\partial \kappa_{xy}}\frac{\partial \kappa_{xy}}{\partial \kappa_x} + \frac{\partial U}{\partial \kappa_y}\frac{\partial \kappa_y}{\partial \kappa_x} \tag{41}$$

Because $\partial U/\partial \kappa_{xy} = 0$, and $\partial U/\partial \kappa_y = 0$, we find

$$M = \frac{\partial U}{\partial \kappa_x} = \frac{Ehb^5}{720}\left[-\kappa_{xy}^2\kappa_y + \kappa_x\kappa_y^2\right] + Db\left[\kappa_x + \nu(\kappa_y - \kappa_{y0})\right] \tag{42}$$

Substituting for κ_y from Eq. (38) into Eq. (40), and solving for zero torque, we obtain after some manipulation:

$$\left[\kappa_{xy}^2 + \kappa_x^2 - \kappa_x\kappa_{y0} + \frac{(1-\nu)}{K}\right]\kappa_{xy} = 0 \tag{43}$$

Thus, either $\kappa_{xy} = 0$, in which case the applied moment, Eq. (41), marginally simplifies

$$M = \frac{Ehb^5}{720}\kappa_x\kappa_y^2 + Db\left[\kappa_x + \nu(\kappa_y - \kappa_{y0})\right] \tag{44}$$

or κ_{xy} is not equal to zero but given by

$$\kappa_{xy}^2 = -\kappa_x^2 + \kappa_x\kappa_{y0} - \frac{1-\nu}{K} \tag{45}$$

The quadratic form has two roots and therefore captures the onset and recession of torsional buckling. For real values of κ_{xy}, we can determine the corresponding values of κ_x, now written in non-dimensional form

$$(\kappa_x r)^2 - \kappa_x r + \frac{60\beta^2}{(1+\nu)} = 0 \tag{46}$$

which is nearly identical to the approximation of Mansfield's solution, Eq. (19), but lacking ν in the quadratic term coefficient. The roots are given by

$$\kappa_x r = \frac{1}{2} \pm \frac{1}{2}\sqrt{1 - \frac{240\beta^2}{(1+\nu)}} = (\kappa_x r)_1, (\kappa_x r)_2 \tag{47}$$

Real roots sets a positive discriminant in Eq. (47), which gives a requirement

$$\beta \leq \sqrt{\frac{1+\nu}{240}} \tag{48}$$

During the torsional buckling phase which prevails when $(\kappa_x r)_1 < \kappa_x r < (\kappa_x r)_2$, we can solve for M by first noting that κ_y greatly simplifies upon substitution of κ_{xy}^2, Eq. (45), into Eq. (38):

$$\kappa_y = \frac{K\kappa_x^2(\kappa_{y0} - \kappa_x) - (1-\nu)\kappa_x - \nu\kappa_x + \kappa_{y0}}{\left[K\kappa_x^2 + 1\right]} \qquad (49)$$

$$\kappa_y = \kappa_{y0} - \kappa_x$$

Substituting for κ_{xy}^2, Eq. (45), and κ_y above into Eq. (42), and making dimensionless, yields

$$\frac{Mr}{Db} = 1 - \nu \qquad (50)$$

This is close to Mansfield's exact solution, albeit lacking the slight negative gradient observed in Fig. 3, and captured in the approximation of Mansfield's moment, Eq. (23). Indeed, it is equivalent to the limiting expression when $\bar{\kappa}_x$ becomes large, Eq. (26).

4.2.3. Second approximation—Solution UC2

The onset of torsional buckling is typically at small κ_x, where there is relatively little cross-sectional deformation; as a further approximation, we set $\kappa_y = 1/r$, as performed by Wang et al. (2019) for orthotropic tape-springs: here, we replicate for isotropic tapes for reference. The total strain energy is now shortened

$$U = Eh\left[\kappa_{xy}^4\frac{b^5}{1440} - \kappa_{xy}^2\kappa_x\frac{b^5}{720r} + \kappa_x^2\frac{b^5}{1440r^2}\right] + \frac{1}{2}Db\left[\kappa_x^2 + 2(1-\nu)\kappa_{xy}^2\right] \qquad (51)$$

The applied torque, T, is given by

$$T = \left(\frac{dU}{d\kappa_{xy}}\right)_{\kappa_x} = \frac{\partial U}{\partial \kappa_{xy}} = Eh\left[\kappa_{xy}^3\frac{b^5}{360} - \kappa_{xy}\kappa_x\frac{b^5}{360r}\right] + 2Db(1-\nu)\kappa_{xy} \qquad (52)$$

and the applied moment, M, by

$$M = \frac{dU}{d\kappa_x} = \frac{\partial U}{\partial \kappa_x} + \frac{\partial U}{\partial \kappa_{xy}}\frac{\partial \kappa_{xy}}{\partial \kappa_x} = \frac{\partial U}{\partial \kappa_x} = Eh\left[-\kappa_{xy}^2\frac{b^5}{720r} + \kappa_x\frac{b^5}{720r^2}\right] + Db\kappa_x \qquad (53)$$

since there is zero torque, and $\partial U/\partial \kappa_{xy} = 0$, which is served by the condition of zero torque by setting Eq. (52) equal to zero and rearranging

$$\kappa_{xy}\left(\kappa_{xy}^2 - \frac{\kappa_x}{r} + \frac{1-\nu}{K}\right) = 0 \qquad (54)$$

Thus either $\kappa_{xy} = 0$, where the moment is given by

$$M = \frac{Ehb^5}{720r^2}\kappa_x + Db\kappa_x \qquad (55)$$

or

$$\kappa_{xy}^2 = \frac{\kappa_x}{r} - \frac{1-\nu}{K} \qquad (56)$$

where the dimensionless moment is

$$\frac{Mr}{Db} = 1 - \nu + \kappa_x r \qquad (57)$$

This contains an increasing linear term, in contrast to the constant UC1 moment and negative gradient exact Mansfield moment; thus, this approximation is valid only for small κ_x.

For the onset of torsional buckling, real κ_{xy} requires $\kappa_{xy}^2 > 0$, with a corresponding value of κ_x when $\kappa_{xy} = 0$ in Eq. (56)

$$\kappa_x = \frac{r(1-\nu)}{K} \Rightarrow \kappa_x r = \frac{60\beta^2}{(1+\nu)} \qquad (58)$$

which is identical to the linear approximation of the Mansfield solution, and a truncation of solution UC1, Eq. (46), at the linear term.

Note that the condition $\kappa_{xy}^2 > 0$ is always satisfied for some κ_x, and torsional buckling is inevitable for any tape-spring; and remains for all κ_x: vanishing of the torsional mode at larger κ_x is not captured, unlike in solution UC1.

4.2.4. Inextensible limit

As a final approximation we consider the limit of zero thickness, in which the tape-spring behaves in an inextensible manner; i.e., remaining a developable surface. There is, thus, no change in Gaussian curvature, which for a straight tape initially, sets

$$\kappa_{xy}^2 = \kappa_x\kappa_y \qquad (59)$$

There is only bending strain energy: substituting Eq. (59) into Eq. (27) and integrating across the width yields

$$U = \frac{1}{2}Db\left[\kappa_x^2 + 2\nu\kappa_x(\kappa_y - \kappa_{y0}) + (\kappa_y - \kappa_{y0})^2 + 2(1-\nu)\kappa_x\kappa_y\right] \qquad (60)$$

Minimising the above with respect to κ_y leads to

$$\kappa_y = \kappa_{y0} - \kappa_x \qquad (61)$$

Substituting back into Eq. (60), and differentiating with respect to κ_x yields the applied moment, M, written here in dimensionless form:

$$\frac{Mr}{Db} = 1 - \nu \qquad (62)$$

and, finally, into Eq. (59), the twist is given by

$$\kappa_{xy}^2 = \kappa_x\kappa_{y0} - \kappa_x^2 \qquad (63)$$

4.3. Comparison of solutions

To aid discussion, and figure annotation, we utilise the following abbreviations for the different solutions:

- EM — Exact Mansfield solution
- AM1 — Taylor series approximation of Mansfield's Ψ_1 function, retaining the first two terms
- AM2 — As per AM1 but retaining only the first term in the approximation of Ψ_1
- UC1 — Approximation assuming uniform transverse curvature which is allowed to vary as a function of κ_x
- UC2 — Approximation assuming uniform transverse curvature of fixed value $1/r$
- IEL — Approximation assuming fully developable behaviour, i.e. in the inextensible limit

4.3.1. Zero-twist solution

Fig. 7 plots the variation of solution UC1, Eq. (44), alongside the zero-twist exact Mansfield solution, Eq. (9), for a range of β values. Our approximate solution captures the bending response quite well, with best agreement for large β. However, solution UC1 overestimates the peak moment by around 20% for $\beta = 0.01$, which decreases with increasing β, and vice versa: an overestimation is to be expected given that our method is essentially a Rayleigh–Ritz method with a single mode shape.

We have also neglected that the edges are free of transverse bending moment, which in turn requires

$$\kappa_y|_{y=\pm b/2} = \kappa_{y0} - \nu\kappa_x \qquad (64)$$

Setting $\kappa_{xy} = 0$ for now in Eq. (38), the above will be satisfied when $K \to 0$, tantamount to $\beta \to \infty$. The Mansfield solution enforces the boundary condition through a boundary layer in which the κ_y curvature "rises" to the required value, visible as an upturned "lip" along the edges of the spring. Meanwhile, in between the edges, small β tape-springs, for which the stretching strain energy dominates, are inclined to minimise mid-surface strains as much as possible, so the cross-section becomes very flat between the edges while remaining very tightly curved at the edges in a small boundary layer. For large β tape-springs, bending energy dominates, so they are less inclined to flatten in the middle and remain closer to a uniform curvature arc (corresponding to a large boundary layer). Hence, if $\kappa_{xy} = 0$, solution UC1 better approximates the Mansfield solution as β increases. The

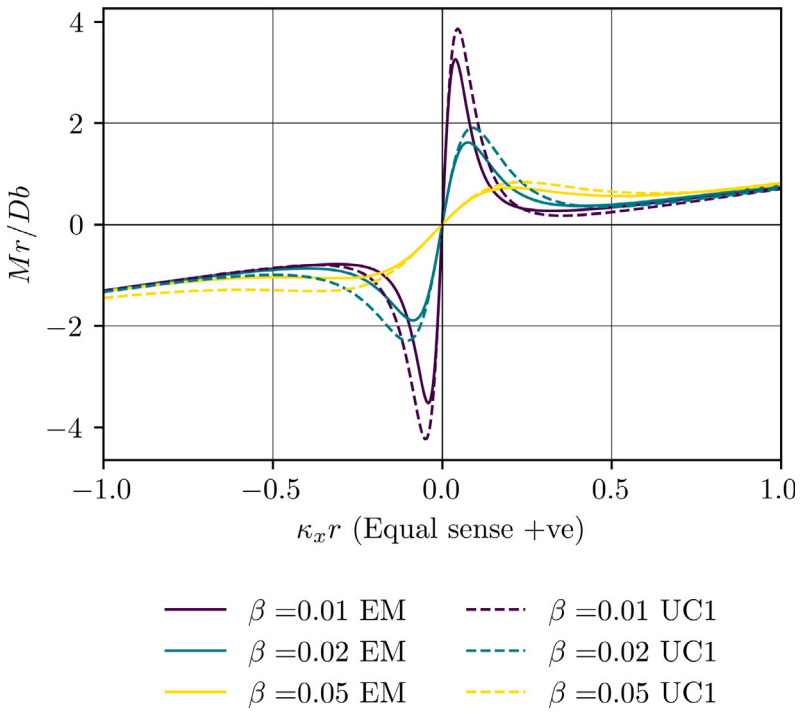


Fig. 7. Solution UC1, Eq. (44), dashed lines, alongside the zero-twist exact Mansfield solution, solid curves, for a range of β.

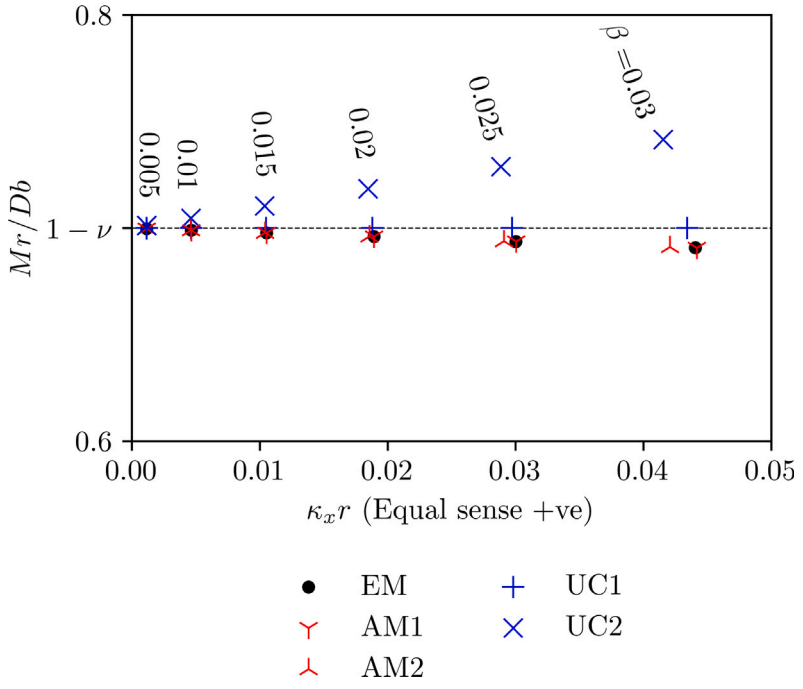


Fig. 8. Onset of torsional buckling.

consideration of torsional buckling alters matters slightly, and a more complete explanation is provided later.

4.3.2. Torsional buckling onset

Fig. 8 plots both uniform curvature approximations, UC1 & UC2, of the onset of torsional buckling, alongside the full Mansfield solution, EM, and Mansfield approximations, AM1 & AM2, for $\nu = 0.3$ (a typical value for metals) and a range of β.

Broadly there is good agreement between the solutions, especially for small β; indeed as $\beta \to 0$ all solutions converge on the inextensible limit: $\kappa_x r = 0$, $Mr/Db = 1 - \nu$. The AM1, AM2 moments are near identical to the exact solution, as is the AM1 curvature, with the AM2 curvature a slight underestimate. Solution UC2 greatly over-predicts the moment at large β, though the predicted curvature is very close to AM2. Solution UC1 performs considerably better than UC2 in terms of predicted moment, and better than both the UC2 *and* AM2 in terms

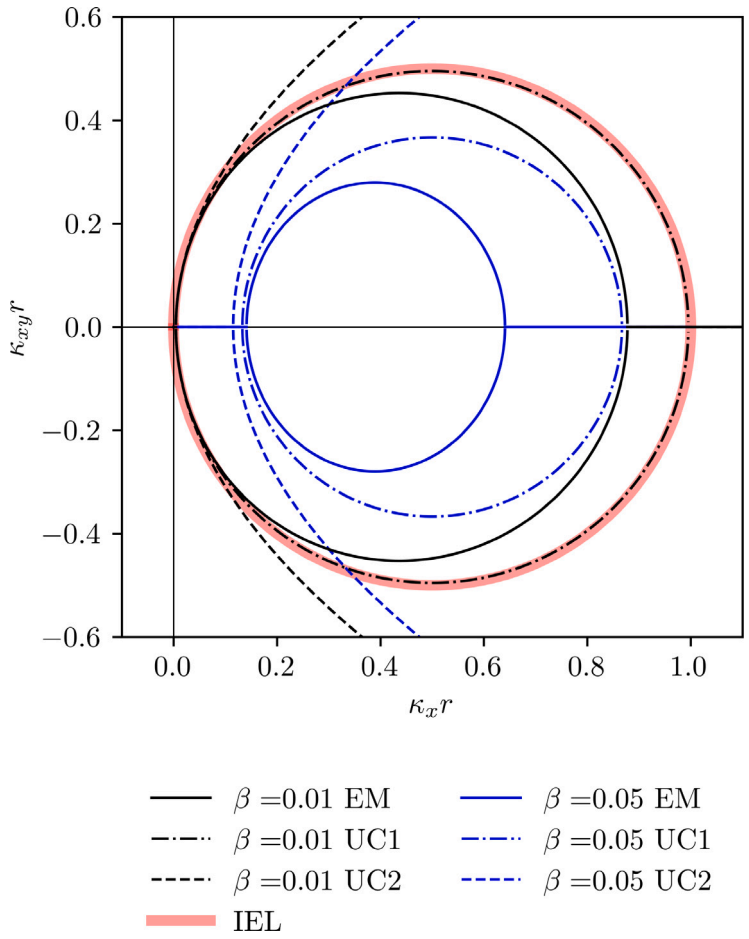


Fig. 9. Exact Mansfield, UC1, & UC2 κ_{xy}, for different β, alongside the inextensible limit. The κ_{xy} circles plotted here can be interpreted as the limits of the unstable energy "bulge" in Figs. 5 & 6, viewed in plan.

of curvature. This is because at large β the torsional buckling occurs at a larger curvature, at which point there is more substantial cross-sectional flattening, decreasing the validity of UC2; and $\bar{\kappa}_x$ is larger, decreasing the accuracy of the single term Taylor series approximation of Ψ_1 in AM2.

4.3.3. Behaviour over larger κ_x

Fig. 9 plots κ_{xy} as a function of κ_x ($\kappa_{xy}r$ vs $\kappa_x r$) for a range of β, in order to compare solution UC1, Eq. (45), and UC2, Eq. (56), to the exact Mansfield expression, Eq. (10). Solutions UC1 & EM only exist over a range of κ_x, which decreases in size as β increases, and eventually vanish. The UC1 onset of torsional buckling agrees closely with the exact Mansfield solution, with agreement decreasing only slightly with larger β; however, as κ_x increases, the solutions diverge, with UC1 suggesting torsional buckling over a greater range of κ_x: solutions diverge for larger β. It can be seen that the Mansfield solution will vanish at a smaller β than solution UC1. The divergent behaviour is again due to edge effects; the UC1 κ_y for the buckled state, given by Eq. (49), exactly satisfies Eq. (64) when $\kappa_x = 0$, and increasingly fails to satisfy as κ_x increases. Solution UC2 agrees reasonably well with UC1 & EM for small κ_x, but completely fails to capture when torsional buckling recedes.

As $\beta \to 0$, Solution UC1, Eq. (45), becomes

$$\kappa_{xy}^2 = \kappa_x(\kappa_{y0} - \kappa_x) \tag{65}$$

which is equal to Eq. (59), the inextensible limit, with trivial roots $\kappa_x = 0$ and $\kappa_x = \kappa_{y0}$, and is also identical to the large $\bar{\kappa}_x$ Mansfield approximation. Thus, the exact Mansfield solution and solution UC1 converge on the inextensible limit, which is a unit-diameter circle in ($\kappa_x r$, $\kappa_{xy} r$) coordinates, plotted as a thick line in Fig. 9, as $\beta \to 0$.

Figs. 10 and 11 plot the equal-sense moment along the stable and unstable paths, as given by the exact Mansfield and UC1 solutions, for equal-sense bending only. As β decreases the EM torsional moment gradually flattens and approaches the inextensible limit, $1 - \nu$, thus converging with UC1.

4.3.4. A paradox

The unbuckled UC1 and exact Mansfield solutions agree better for $\beta \to \infty$ (as per Fig. 7), whilst the buckled UC1 and exact Mansfield solutions agree better for $\beta \to 0$ (Fig. 8): such disparate behaviour presents paradoxical behaviour, which can be resolved by examining Figs. 12 and 13.

Fig. 12 shows Mansfield's exact solution for the transverse curvature, for a range of β, at a given κ_x. For small β, stretching energy dominates, so κ_y takes a constant value across the width which minimises the change in Gaussian curvature, and rises only at the edges to satisfy the boundary condition; the profile is therefore very close to that of a circular arc and the UC1 and Mansfield solutions converge. For large β, bending energy dominates, so the curvature remains close to the required edge curvature—as it is the value of curvature which minimises bending energy alone—across the section. Again, this consistent curvature results in a profile very close to an arc and the UC1 and Mansfield solutions converge. As the tape-spring transitions between these two extremes, the curvature varies more greatly across the section, as can be seen in Fig. 12. Therefore between the two extremes, the curvature is less uniform, and solution UC1 is less valid.

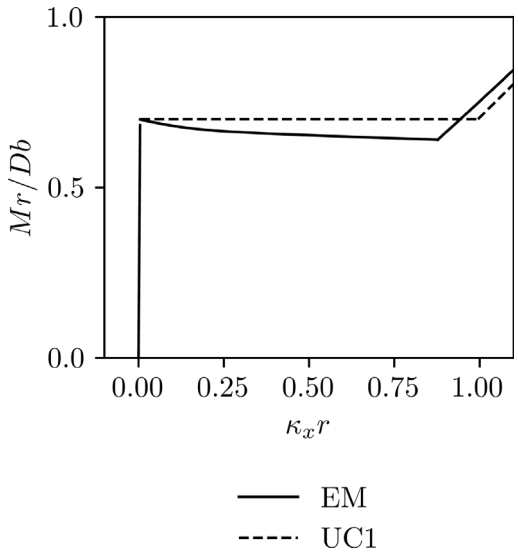


Fig. 10. Exact Mansfield and UC1 moments for $\beta = 0.01$.

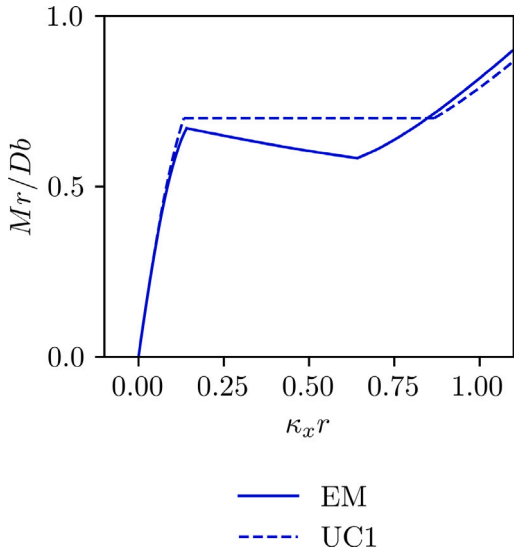


Fig. 11. Exact Mansfield and UC1 moments for $\beta = 0.05$.

To further illustrate the deviation of Mansfield's exact solution from uniform curvature, Fig. 13 plots the standard deviation of the curvature as a function of β for different $\kappa_x r$. If the standard deviation is zero, the transverse curvature must be uniform, and thus the exact and approximate solutions agree. There is a peak evident around $\beta = 0.06$, with the standard deviation decreasing as both $\beta \to 0$ and $\beta \to \infty$. Thus the apparent paradox can now be explained: for torsional buckling, which only occurs below a critical β (indicated by the dashed line in Fig. 13), curvature uniformity, and hence agreement between UC1 and the exact Mansfield solution, increases with decreasing β, whilst, if torsional buckling does not occur, agreement increases with increasing β.

4.3.5. Critical β for torsional buckling to occur

In a final comparison, we compare the existence of torsional buckling in Mansfield's exact solution, Eq. (10), to the UC1 condition, Eq. (48). In terms of the former, we recast Eq. (10), noting it must be larger or equal to zero for torsional buckling to occur, as:

$$\kappa_x r(1 - \nu\kappa_x r) - \frac{16}{3(1+\nu)} \frac{\beta^2}{\Psi_1(\beta, \kappa_x r)} \geq 0 \tag{66}$$

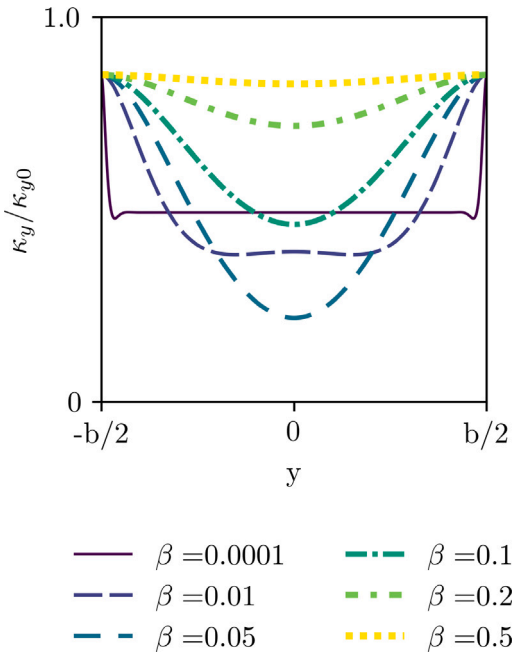


Fig. 12. Mansfield transverse curvature at $\kappa_x r = 0.5$, for varying β. The flatter the curve, the closer the UC1 & EM solutions will agree.

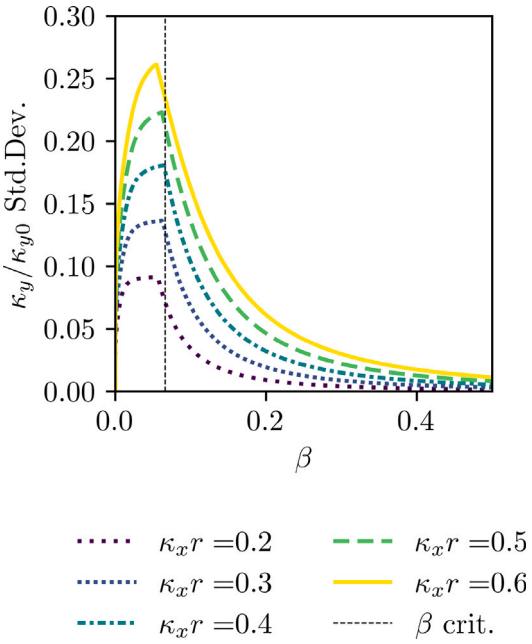


Fig. 13. Standard deviation in Mansfield transverse curvature, at varying $\kappa_x r$ and β.

The left hand side is evaluated over a 2D array of β and $\kappa_x r$: for each β the maximum value of the left hand side, which occurs at some $\kappa_x r$, is recorded to give a 1D array over a range of β. The location at which the left hand side becomes zero then gives the critical β: Fig. 14 plots the corresponding thresholds for β. It can be seen there is fairly good agreement, and, critically, the approximate UC1 solution is conservative, and, thus, provides a good design equation for torsional buckling.

It should be noted that an attempt to use the quadratic Mansfield approximation for $\bar{\kappa}_{xy}^2$ to derive a discriminant condition similar to Eq. (48) leads to

$$\beta \leq \sqrt{\frac{1+\nu}{240\nu}} \tag{67}$$

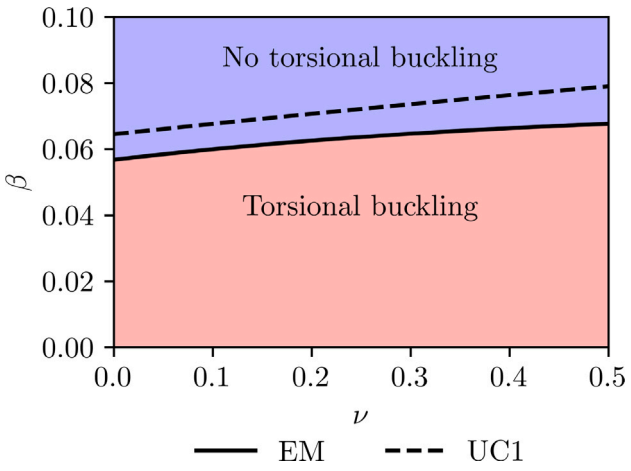


Fig. 14. Torsional buckling threshold.

differing in the appearance of ν in the denominator. For $\nu = 0.3$ this leads to a critical β value 1.8 times the value from Eq. (48); clearly, of no use.

5. Conclusions

A summary of Mansfield's tape-spring analysis has been presented, and the importance of the non-dimensional parameter $\beta = rh/b^2$ discussed. Approximations of Mansfield's hyperbolic functions in the limit of small curvature have led to various closed form predictions of the curvature at which torsional buckling initiates (to varying degrees of accuracy), and a compact approximation for the torsional buckling moment. Likewise, an approximation of the functions in the small thickness limit leads to a prediction of torsional behaviour over the whole range of curvature.

Three alternative solutions which make use of simplifying approximations about the deformed cross-section and capture the equal-sense torsional buckling have been presented: all have a uniform transverse curvature. First, solution UC1 assumes that the transverse curvature takes a value which minimises the strain energy, thus capturing flattening of the cross section and remaining valid for all κ_x. A second approximation, UC2, noting that the onset of torsional buckling occurs at small curvatures, assumes the transverse curvature remains unchanged from its original value, $1/r$. Finally the inextensible limit is considered, in which the behaviour is fully developable.

Solution UC1 provides a closed form quadratic which can be solved to find the range of κ_x over which torsional buckling occurs, and the non-dimensional torsional buckling moment is shown to be $1 - \nu$, both agreeing closely with Mansfield's solution. UC1 also provides a condition on β for torsional buckling to occur; this is compared to the numerically evaluated Mansfield criteria and found to be a close conservative approximation. Solution UC2 gives a reasonable approximation for the onset of torsional buckling but is only valid for small κ_x.

It is shown that solutions UC1, UC2, and the exact Mansfield solution converge on the inextensible limit as $\beta \to 0$. Additionally, it is shown that solution UC1 converges on the Mansfield solution as $\beta \to \infty$, and a physical interpretation of this convergence is discussed.

Interestingly, the torsional buckling moment in the inextensible limit is equal to the fold moment of a tape-spring in equal-sense bending, suggestive of a fundamental link between the two instabilities. Indeed, this highlights a limitation of our approximate solutions, which are smooth, and cannot account for the two-phase curvature of a folded tape-spring. In practice, in equal-sense bending, folding initiates long before the recession of the torsional mode suggested by Fig. 9. Predicting the curvature, and manner in which a tape-spring transitions from twisted to folded, is of great practical interest. Our paper Clarkson and Seffen (2024), currently in review, aims to develop the understanding of tape-spring folds in the context of elastic localisation; the interaction between torsion and folding is a topic certainly worthy of further study.

Though not as accurate as Mansfield's exact analytical solution, the approximate solutions presented in this paper are much less unwieldy, and it is envisaged they may find use in early stage "back of the envelope" calculations during the design of tape-spring deployable structures. Additionally, the relative simplicity of expression means they can be readily extended to problems where deformation is *not* uniform in the lengthwise direction, such as the question of the torsional buckling mode shape—currently under investigation by the authors.

CRediT authorship contribution statement

J.A. Clarkson: Writing – review & editing, Writing – original draft, Methodology, Investigation, Formal analysis. **K.A. Seffen:** Writing – review & editing, Supervision, Conceptualization.

Declaration of competing interest

The authors declare that they have no known competing financial interests or personal relationships that could have appeared to influence the work reported in this paper.

Data availability

No data was used for the research described in the article.

Acknowledgements

The authors would like to thank the EPSRC and Structure Mode for funding this research through the EPSRC Centre for Doctoral Training in Future Infrastructure and Built Environment: Resilience in a Changing World (EPSRC grant reference number EP/S02302X/1).

References

Audoly, B., Neukirch, S., 2021. A one-dimensional model for elastic ribbons: a little stretching makes a big difference. J. Mech. Phys. Solids 153, 104457.

Batdorf, S.B., 1947. A Simplified Method of Elastic-Stability Analysis for Thin Cylindrical Shells. National Advisory Committee for Aeronautics, https://ntrs.nasa.gov/citations/19930091945.

Brazier, L.G., 1926. The flexure of thin cylindrical shells and other thin sections. In: Reports & Memoranda Number 1081, vol. 11, British Aircrsft Research Council.

Calladine, C.R., 1983. Theory of Shell Structures. Cambridge University Press.

Calladine, C.R., Seffen, K.A., 2020. Folding the carpenter's tape: Boundary layer effects. J. Appl. Mech. 87 (1), 011009–1–5.

Clarkson, J.A., Seffen, K.A., 2024. Elastic localisation with particular reference to tape-springs. in review.

Galletly, D.A., Guest, S.D., 2004. Bistable composite tubes. II. A shell model. Int. J. Solids Struct. 4503–4516.

Guest, S.D., Pellegrino, S., 2006. Analytical models for bistable cyindrical shells. Proc. R. Soc. Lond. A 462, 839–854.

Iqbal, K., Pellegrino, S., Daton-Lovett, A., 2000. Bi-Stable Composite Slit Tubes, Proceedings of IUTAM-IASS Symposium on Deployable Structures. 6–9 September 1998, Kluwer Academic Publishers, pp. 153–162,

Kumar, A., Audoly, B., Lestringant, C., 2023. Asymptotic derivation of a higher-order one-dimensional model for tape springs. Phil. Trans. R. Soc. A 381 (2244), 20220028.

Mansfield, E.H., 1973. Large-deflexion torsion and flexure of initially curved strips. Proc. R. Soc. Lond. A 334 (1598), 279–298.

Miura, K., Pellegrino, S., 2020. Forms and Concepts for Lightweight Structures. Cambridge University Press.

Rimrott, F.P.J., 1965. Storable tubular extendible member: a unique machine element. Mach. Des. 37 (28), 156–165.

Rimrott, F.P.J., 1970. Querschnittsverformung bei torsion offener profile. ZAMM Z. Angew. Math. Mech. 50 (12), 775–778.

Seffen, K.A., 2009. 'Morphing' bistable orthotropic elliptical shells. Proc. R. Soc. Lond. A 463 (2077), 67–83.

Supple, W.J., 1969. Initial post-buckling behaviour of a class of elastic structural systems. Int. J. Non-Linear Mech. 4 (1), 23–36.

Thompson, J.M.T., Hunt, G.W., 1973. A General Theory of Elastic Stability. John Wiley and sons.
Thornton, E.A., Eby, D.L., Chung, P.W., 1998. Torsional buckling of the hubble space telescope solar arrays. Int. J. Space Struct. 13 (2), 65–74.
Vidoli, S., Maurini, C., 2008. Tristability of thin orthotropic shells with uniform initial curvature. Proc. R. Soc. Lond. A 464 (2099), 2949–2966.
Wang, B., Seffen, K.A., Guest, S.D., 2019. Folding of bistable composite tape-springs. CUED/D-STRUCT/TR.252.
Wuest, W., 1954. Einige Anwendungen der Theorie der Zylinderschale. ZAMM Z. Angew. Math. Mech. 34 (12), 444–454.